J Nanopart Res (2009) 11:995–1003
DOI 10.1007/s11051-008-9550-5

BRIEF COMMUNICATION

Synthesis and characterization of titanium nitride, niobium nitride, and tantalum nitride nanocrystals via the RAPET (reaction under autogenic pressure at elevated temperature) technique

P. P. George · A. Gedanken · Shirly Ben-David Makhlouf · I. Genish · A. Marciano · Riam Abu-Mukh

Received: 5 June 2008 / Accepted: 22 October 2008 / Published online: 29 November 2008

Abstract TiN, NbN, and TaN nanocrystals have been selectively prepared through a simple, solvent-free, and convenient reaction under autogenic pressure at moderate temperature (RAPET) process at 350 °C for 12 h, reacting transition metal chlorides and sodium azide. The nanostructures obtained are characterized by powder X-ray diffraction (PXRD), transmission electron microscopy (TEM), and scanning electron microscopy (SEM). A reaction mechanism is suggested based on the experimental results. These rapid reactions produce nanocrystals of TiN, NbN, and TaN with average sizes of approximately 30, 28, and 27 nm, respectively (as calculated from X-ray line broadening). An octahedral inorganic fullerene was detected among the various structures of the TiN.

Keywords Metal nitrides · Nanoparticles · Inorganic fullerenes · Particle production

P. P. George · A. Gedanken (✉) · S. B.-D. Makhlouf · I. Genish · A. Marciano · R. Abu-Mukh
Department of Chemistry, Kanbar Laboratory for Nanomaterials, Institute of Nanotechnology and Advanced Materials, Bar-Ilan University, Ramat-Gan 52900, Israel
e-mail: gedanken@mail.biu.ac.il

Introduction

Motivated by the novel applications of diverse nanometer-scale materials, extensive research has been carried out on the design and preparation of nanostructures with different shapes and sizes because of their corresponding novel properties and potential uses (Buha et al. 2007; Gomathi and Rao 2006; Zhang and Gao 2004; Fischer et al. 2007; Wu et al. 2005). Recently, the preparation of group four (for example, TiN) and group five (for example, NbN and TaN) transition metal nitrides has attracted extensive attention among synthetic chemists owing to their special physical and chemical properties. They exhibit metallic conductivity and some show superconductivity (Toth 1971; Storms 1972; Joshi et al. 2005; Hu et al. 2000). These nitrides are generally resistant to chemical attack and are stable at high temperatures under inert or reducing atmospheres (Blocher 1956). The important applications of these materials are as hard, protective coatings for cutting tools (Buhl et al. 1981; Sundgren 1985). Dense crucibles of ZrN and TiN serve as vessels for the melting of metal. Recently, the superconductivity of NbN has been exploited to make superconducting coatings in radiofrequency cavities (Fabbricatore et al. 1989), and TiN has shown promising results as a diffusion barrier for microelectronics (Ostling et al. 1986; Gillan and Kaner 1994). Tantalum nitride coatings are used in electronics industry as a diffusion barrier (Aryasomayajula et al. 2006). Niobium nitride

thin films can be used for corrosion protective applications (Fenker et al. 2003). Recently, Serro et al. studied the TiN films for biomedical applications (Gispert et al. 2007).

There are several methods quoted in the literature for the preparation of metal nitrides (Carmalt et al. 2003; Tenne et al. 1992; Margulis et al. 1993; Tenne 1995; Troitskiy et al. 2003; Li and Gao 2003; O'Loughlin et al. 2001). In the current article, single-crystalline wide band gap semiconductors, TiN, NbN, and TaN nanocrystals, are prepared by using a mixture of metal chlorides and sodium azide via a convenient low temperature *r*eaction under *a*utogenic *p*ressure at *e*levated *t*emperature (RAPET) technique. There is only one reference that reports the synthesis of titanium nitride at ambient temperature (Griffiths et al. 2001). From the literature search, this is the lowest temperature ever reported for the fabrication of NbN and TaN nanocrystals. The RAPET approach used for the fabrication of TiN, NbN, and TaN is uncomplicated, solvent less, and environment friendly. We had employed the RAPET technique for nitride formation, emphasizing the relatively low temperature under which these nitrides are prepared.

Experimental

Reagents

$TiCl_4$, $NbCl_5$, $TaCl_5$ (Aldrich, 99.9%), and NaN_3 (Sigma, anhydrous) used as-received.

Synthesis

The synthesis of TiN, NbN, and TaN nanocrystals was carried out by the thermal decomposition of a mixture of $TiCl_4$ and NaN_3, purchased from Aldrich Co. and used as-received. The 3-mL closed vessel cell was assembled from stainless steel Letlok parts (manufactured by HAM-LET Co., Israel). A $^1/_2''$ union part was plugged from both sides by standard caps. For the synthesis, 0.25 mL of $TiCl_4$ and 0.59 g of NaN_3 were introduced into the cell at room temperature. The filled cell was closed tightly by the other plug and then placed inside an iron pipe in the middle of the furnace. The temperature was raised at a heating rate of 10 °C/min. The closed-vessel cell was heated at 350 °C for 12 h. The reaction took place under the autogenic pressure of the precursors. The Letlok was gradually cooled ($\sim$1–2 h) to room temperature, and after opening a mixture of brown powder and white salt was obtained. We have followed the above synthetic strategy for the synthesis of NbN and TaN nanomaterials by the RAPET method. For the synthesis of NbN, 0.4 g of $NbCl_5$ and 0.5 g of NaN_3 were introduced into the cell at room temperature. For the synthesis of TaN, 0.2 g of $TaCl_5$ and 0.18 g of NaN_3 were introduced into the cell at room temperature The as-prepared products synthesized through RAPET synthesis were further washed with water and diluted HCl in order to remove the NaCl. The washing removes the NaCl and leads to the formation of neat TiN, NbN, and TaN nanocrystals. The experimental results are summarized in Table 1.

Warning

Exceeding this amount of reactants inside the 3-mL capacity of the stainless steel Letlok is not advisable. In other words, care should be taken to perform these solid-state metathesis reactions on a small scale first (less than 1 g of reactant mixture), taking adequate

Table 1 Summary of experimental data, including reaction temperature and times, material color, the identity of the structure comprising the reaction product after washing the as-prepared material with diluted HCl and distilled water

Ratio of starting materials[a]	Reaction temperature (°C) and time (h)	Product[b] and material color	Morphology
$TiCl_4 + NaN_3$ (1:4)	350 °C–12 h	TiN–brown	Nanocrystals
$NbCl_5 + NaN_3$ (1:5)	350 °C–12 h	NbN–black	Nanocrystals
$TaCl_5 + NaN_3$ (1:5)	350 °C–12 h	TaN–black	Nanocrystals

[a] Prepared via the RAPET technique

[b] Crystalline products obtained via washing the as-prepared samples with water and diluted HCl

safety precautions. The Letlok parts are not dangerous to open it after the reaction.

Characterization

The XRD patterns of TiN, NbN, and TaN samples are recorded using a Bruker D8 diffractometer with Cu Kα radiation. C, H analysis was carried out on an Eager 200 CE instrument and an EA 1110 Elemental Analyzer. The morphologies of the as-prepared sample are studied by a scanning electron microscope (SEM), and SEM coupled with energy dispersive X-ray analysis (EDX). Transmission electron microscopy (TEM) studies are carried out on a JEOL 2000 electron microscope. High-resolution TEM (HRTEM) images are taken using a JEOL 2010 with a 200-kV accelerating voltage. Samples for the TEM and HRTEM measurements are obtained by placing a drop of the suspension from the as-sonicated reaction product in ethanol onto a carbon-coated copper grid, followed by drying under air to remove the solvent. Energy-dispersive X-ray analysis (EDX) studies are carried out on a JEOL micrograph (JEOL 2010 operated at 200 kV).

Results

Powder X-ray diffraction (PXRD), elemental (C and H) analysis, SEM, TEM, HRTEM, and EDX analysis

The PXRD patterns of the thermally decomposed mixture of MCl_n [M = Ti, Nb and Ta; $n = 4$ or 5] and NaN_3 at 350 °C in a closed Letlok cell under air atmosphere are presented in Fig. 1a–c.

The elemental (C, H, N, S) analysis detected 0% carbon and 0% hydrogen in the TiN, NbN, and TaN products after the washing process. The calculated elemental (wt) percentages of N, Ti, Na, and Cl in the mixture of $TiCl_4$ and NaN_3 before a reaction are 16%, 17%, 9.2%, and 56%, respectively. We could determine the nitrogen content in the TiN sample with an elemental [C, H, N, and S] analyzer. The measured amount of nitrogen in the three samples, TiN, NbN, and TaN, are 21 wt% (theoretically 23%), 13 wt% (theoretically, 14%), and 8 wt% (theoretically 8%), respectively. The XRD analyses of the three metal nitride nanocrystals are shown in Table 2.

The morphologies of titanium nitride, niobium nitride, and tantalum nitride crystals

The morphologies of the TiN, NbN, and TaN nanocrystals are observed by SEM, TEM, and HRTEM analysis. The morphologies of the neat TiN nanocrystals obtained after washing the as-prepared sample with water and diluted HCl under air atmosphere are primarily investigated by SEM measurements. Figure 2a demonstrates the SEM image of neat TiN crystals. The neat TiN sample shows various morphologies, including nanocrystals, a few crystals, as well as disordered nanoplate particles. The mean diameter of the various nanosized particles is ~180 nm. The stacking of two or more nanocrystals is also observed in the SEM picture. The diameter of the sintered TiN nanocrystals varies in the range of 250–350 nm. In addition to the nanocrystals there are disordered plates, and the size of these nanoparticles varies in the range of 350–600 nm in diameter. Gillan et al. demonstrated the synthesis of cupric nitride nanoparticles with nearly cubic shape morphology via a solvothermal route (Choi and Gillan 2005).

Figure 2b demonstrates the SEM image of neat NbN nanocrystals obtained after washing the as-prepared NbN sample with a diluted HCl aqueous solution. Although many of the nanocrystals are still observed in the SEM picture (Fig. 2b), the disordered nanosheets are also detected along with the nanocrystals. The size of the NbN nanocrystals varies in the range of 80–90 nm in diameter. The stacking of two or more nanocrystals, and nanosheets, also appears in the SEM image. This type of typical assembly might be due to the sintering of the nanoparticles. The diameter of the sintered NbN nanoparticles varies in the range of 230–350 nm.

Figure 2c demonstrates the SEM images of TaN nanocrystals. The washed sample shows crystalline particles. The diameter of the crystalline particles is in the range of 200–500 nm. In addition to the nanocrystals in the washed product, we have found a fine powder with a morphology suggestive of agglomerations of hundreds of small spherical nanoparticles. The diameter of the agglomerates is in the range of 280–570 nm. EDX measurements carried out on individual TiN, NbN, and TaN nanocrystals of samples washed with diluted HCl and water indicate the presence of only Ti/N, Nb/N, and Ta/N, respectively, and no other impurities

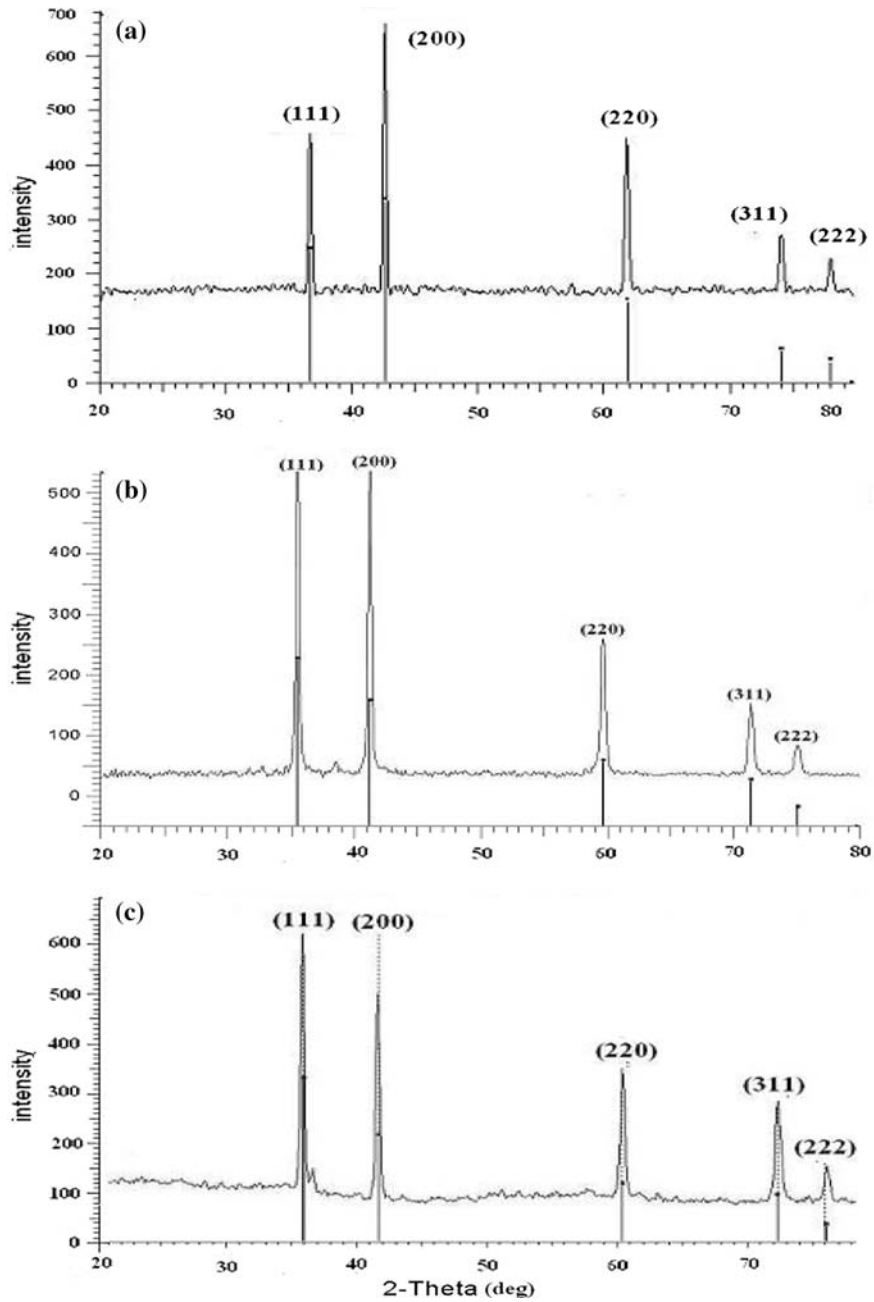

Fig. 1 PXRD pattern of the thermally decomposed mixture of **a** $TiCl_4 + NaN_3$, **b** $NbCl_5 + NaN_3$, and **c** $TaCl_5 + NaN_3$ at 350 °C under air atmosphere and further washed with water and diluted HCl

are detected. The M/N, atomic ratio in the MN [M = Ti, Nb, and Ta] nanocrystals, obtained from EDX analysis is ~1:1, which is in agreement with the MN formula.

The particle sizes of TiN, NbN, and TaN nanocrystals calculated by the X-ray measurements are smaller than that of calculated by the SEM measurements. Aggregation of small particles is responsible for these discrepancies.

TEM and HRTEM measurements

The structures of the TiN, NbN, and TaN nanocrystals are further studied by TEM and HRTEM measurements. The TEM image of TiN nanocrystals is illustrated in Fig. 3a. The TiN nanocrystals have dimensions in the range of 100–350 nm.

The TEM image reveals that at least small parts of the TiN nanoparticles are formed in a cubic shape,

Table 2 The obtained products, crystal structure, morphology, and lattice parameters are illustrated

Nitride sample	Sample phase	Particle size[c] (nm)	JCPDS card no.	Lattice parameters *a* in A
TiN[a]	FCC[b]	32	1-71-299	4.22
NbN[a]	FCC[b]	28	1-89-5128	4.38
TaN[a]	FCC[b]	27	1-89-5196	4.31

[a] Prepared via the RAPET technique

[b] All products are crystallized in face-centered cubic structure

[c] Average particle sizes of TiN, NbN, and TaN are estimated from PXRD line-broadening employing the Scherer formula

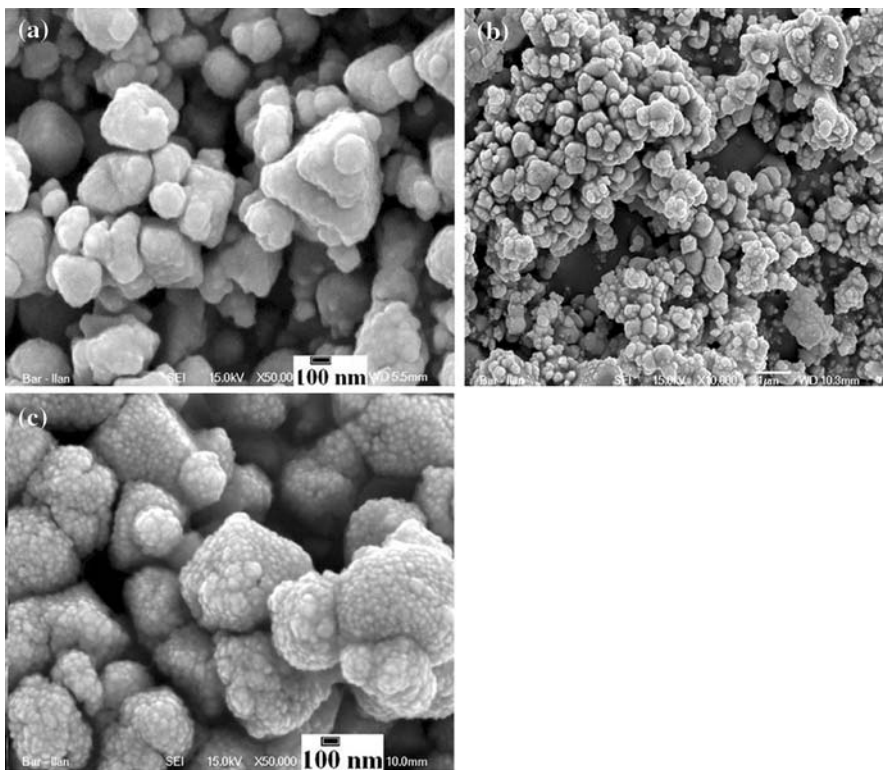

Fig. 2 **a** SEM images of TiN nanocrystals obtained after washing the as-prepared sample with water and a diluted HCl aqueous solution. **b** SEM images of NbN nanocrystals. **c** SEM images of TaN nanocrystals obtained after washing the as-prepared sample with water and diluted HCl

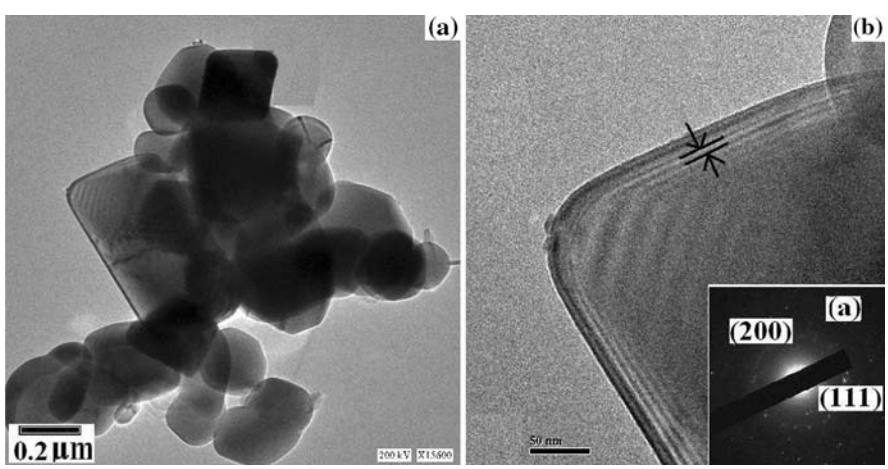

Fig. 3 **a** TEM image of TiN nanocrystals obtained after washing the as-prepared sample with water and diluted HCl aqueous solution. **b** HRTEM image of the edge portion of one individual TiN nanocrystal with diffraction pattern (*inset* (a))

while the rest are crystalline particles. The TiN nanocrystals obtained by RAPET differ from the spherical-shaped TiN nanoparticles obtained by Rao's synthetic strategy (Gomathi and Rao 2006). Rao and coworkers have designed and synthesized spherical TiN nanoparticles by the reaction of $TiCl_4$ with urea using an acetonitrile solvent, and the reaction was maintained in an autoclave at 900–1,000 °C for 3 h in N_2 atmosphere. Our experimental approach in this article involves a similar precursor, $TiCl_4$, which requires neither solvents nor a nitrogen atmosphere for the formation of TiN nanocrystals. The TiN nanocrystals produced under Letlok reaction conditions have lengths ranging from 160 to 350 nm and are larger than those of the TiN nanoparticles (25 nm) produced by Rao's synthetic approach. Perhaps each of these larger structures is an agglomerate of 30 nm particles, a number calculated by PXRD for the particle's size.

In order to obtain the detailed structure and composition of individual TiN, NbN, and TaN nanocrystals, we have carried out a HRTEM image, selected area electron diffraction (SAED), and selected area energy dispersive X-ray spectroscopy (SAEDS) measurements. Figure 3b demonstrates the HRTEM image of the edge of a single octahedral TiN nanocrystal. The measured distance between the fringes is 3.8 nm which is of course much larger than the planes separation of the face-centered cubic lattice of the TiN. Therefore, the unique TiN shape exhibited in Fig. 3a and b is interpreted as an inorganic fullerene (IF)-like structure. The first IFs, MoS_2, and WS_2 were discovered by Tenne et al. They have shown that triangular and rectangular onion-like shapes exist (Hershfinkel et al. 1994). Although bulk synthesis of the IFs normally yields quasi-spherical nanoparticles with at least 20 molecular layers and outer diameters of greater than 30 nm, the formation of hollow MoS_2 clusters with octahedral or tetrahedral shapes was often observed (Tenne et al. 1992; Margulis et al. 1993; Tenne 1995). We observe in the TiN structure at least six molecular layers and more are perhaps hidden. The corresponding SAED pattern is demonstrated in inset (a) of Fig. 3b, featuring a single crystalline TiN. In order to identify the composition of nanocrystals, we have measured a selected area EDS analysis of an individual TiN crystalline particle (figure not represented here). The measurements demonstrate the existence of 78.4 wt% of Ti and 22.5 wt% of N, which is very close to the theoretical value of TiN (Ti = 77 wt% and N = 23 wt%).

Figure 4 depicts the TEM image of the morphology of the neat NbN particles. Nanocrystals are the major structure observed in the picture. They are obtained after washing the as-prepared product with water and a diluted HCl aqueous solution. The face of the neat NbN nanocrystals has a length in the range of 75–100 nm. The average size of the agglomerated nanocrystals is 205 nm.

Figure 4b demonstrates the HRTEM image of the edge of a single NbN nanocrystal. The image is

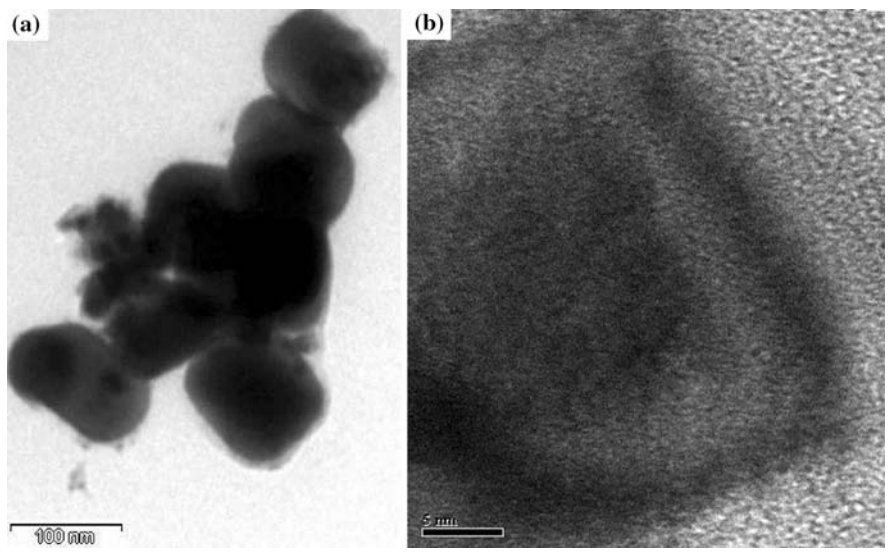

Fig. 4 **a** TEM image of NbN nanocrystals obtained after washing the as-prepared sample with water and a diluted HCl aqueous solution. **b** HRTEM image of the edge portion of one individual NbN nanocrystal with diffraction pattern (*inset* (a))

recorded along the [111] zone. The measured distance between these (111) lattice planes is 0.22 nm, which is very close to the distance between the planes reported in the literature (0.25 nm) for the face-centered cubic lattice of the NbN [powder diffraction file (PDF) no. 01-089-5128]. The corresponding SAED pattern is demonstrated in inset (a) of Fig. 4b, featuring a single crystal of NbN nanocrystals.

Figure 5 represents the TEM image of TaN nanocrystals. The TEM image shows the agglomerated TaN nanocrystals. The TaN nanocrystals are the major structure observed in the picture and have an average diameter in the range of 25–65 nm. The diameter of the agglomerated spherical nanocrystals is in the range of 150–180 nm.

Inset (a) of Fig. 5 demonstrates the HRTEM image of a single TaN nanocrystal. The image is recorded along the [111] zone. The measured distance between these (111) lattice planes is 0.23 nm, which is very close to the distance between the planes reported in the literature (0.25 nm) for the face-centered cubic lattice of the TaN [powder diffraction file (PDF) no. 01-089-5196].

Discussion

The mechanism suggested herein was based on the obtained analytical data and also on previously published data. From XRD, EDX, elemental (C, H, N, S) analysis, SEM, TEM, and HRTEM analysis, it was clear that the product, i.e., MN (M = Ti, Nb and Ta) nanocrystals, is obtained as a result of the RAPET reaction of $TiCl_4$ and NaN_3 under Letlok reaction conditions. The Letlok cell in our reaction is heated to a temperature of 350 °C, which is sufficiently hot to start a reaction between metal chlorides and azide (Gillan and Kaner 1994). The NaN_3 decomposes to Na and N_2 at 365 °C (Gillan and Kaner. 1994). The boiling points of $TiCl_4$, $NbCl_5$, and $TaCl_5$ used in this study are 137, 254, and 242 °C, respectively, and these precursors decompose to metals and chlorine atoms below 500 °C. As the heating continues, the thermal decomposition of reactants (Eq. 1) takes place producing transition metal, Na, Cl, and N atoms in the gaseous phase. The second step involves the initial formation of the by-product, salt, with a reaction between chlorine and sodium, followed by a reaction of finely divided metal and nitrogen gas in a molten salt flux, as shown in Eq. 2. In the second step, the thermodynamically favored by-product, NaCl, serves as a potent driving force, enhancing the nitride formation process (Gillan and Kaner 1994).

$$MCl_x + xNaN_3 \rightarrow M + Na + nN_2 + nCl_2 \quad [x = 4,\ 5] \tag{1}$$

$$M + Na + nN_2 + nCl_2 \rightarrow MN + NaCl \tag{2}$$

Previously, Kaner and coworkers had initiated the solid-state metathesis reaction between metal chlorides (M = Ti, Nb, and Ta) and NaN_3 or Li_3N by

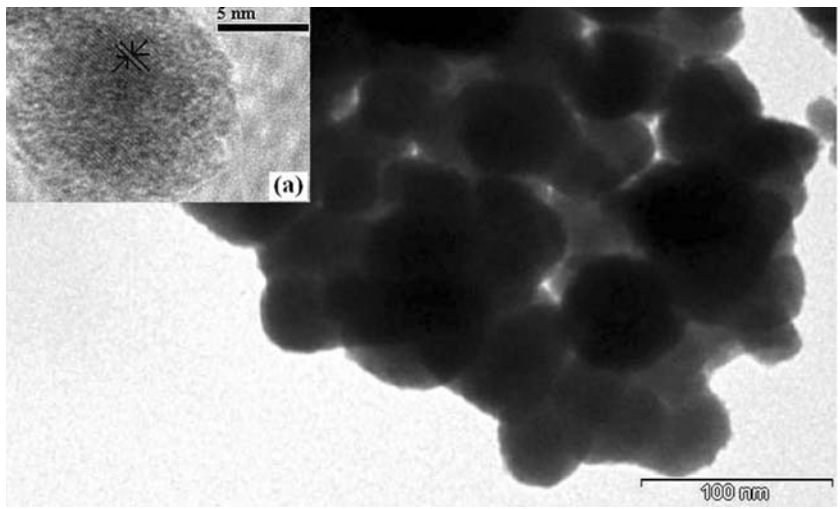

Fig. 5 TEM image of TaN nanocrystals obtained after washing the as-prepared sample with water and a diluted HCl aqueous solution. *Inset* (a) of this figure demonstrates the HRTEM image of one spherical TaN nanocrystal

employing the hot filament for a few seconds producing the metal nitrides, MN (Gillan and Kaner 1994). Parkin had filled the metal chloride and sodium azide into the Pyrex ampoule and heated the ampoule in the furnace in the temperature range of 300–400 °C for the production of metal nitrides (Hector and Parkin 1995). However, the RAPET reaction reported in this article was operated at 350 °C. The variety of RAPET reactions addressed in references (George et al. 2007; George and Gedanken 2008; Pol et al. 2004a, b, c, 2006) generates nanocrystals with distinct morphologies. It is evident that the growth of one-, two-, and three-dimensional nanostructures, such as nanorods, nanotubes, nanofilms, 3-D nanorods, 3-D nanotubes, and 3-D nanofibers, occurs under the influence of temperature and pressure. Similarly, we suggest that under the application of autogenic pressure, the metathesis reaction can be conducted at a lower temperature due to the high pressure of N_2 and Cl_2 pushing the reaction towards products. In addition, the low temperature favors the formation of TiN and NbN nanocrystals. In the current study, the RAPET technique yielded a 76%, 92%, and 96% (wt) recovery of the starting reaction mixture for TiN, NbN, and TaN, respectively.

Conclusions

In summary, by adjusting the metal halides to the sodium azide ratio, the temperature, and the reaction time, a series of metal nitrides (TiN, NbN, and TaN) can be selectively synthesized in the absence of a solvent, a catalyst, or surfactant through a convenient, low temperature RAPET method. This work is valuable for the understanding of the formation of metal nitrides via a simple, convenient, and low temperature RAPET technique. This article has provided a general and effective method to control the composition and phase structure of transition metal nitrides, which will be very important for inorganic synthesis methodology and further applications of metal nitrides.

Acknowledgments P. P. George thanks the Bar-Ilan Research authority for a post-doctoral fellowship and also thanks Dr. Tova Tamari, Dr. Judith Grinblat, Dr. Yuri Koltypin, Ms. M. Shirly, and Mr. Avi Marciano for their help with TEM, HRTEM measurements, technical support, XRD diffraction patterns, and diffuse reflectance spectroscopy, respectively.

References

Aryasomayajula A, Valleti K, Aryasomayajula S, Bhat DG (2006) Pulsed DC magnetron sputtered tantalum nitride hard coatings for tribological applications. Surf Coat Technol 201:4401–4405

Blocher JM (1956) Nitrides. In: Campbell IE (ed) High temperature technology. Wiley, New York, p. 171

Buha J, Djerdj I, Antonietti M, Niederberger M (2007) Thermal transformation of metal oxide nanoparticles into nanocrystalline metal nitrides using cyanamide and urea as nitrogen source. Chem Mater 19:3499–3505

Buhl R, Pulker HK, Moll E (1981) TiN coatings on steel. Thin Solid Films 80:265–270

Carmalt CJ, Dinnage CW, Parkin IP, Peters ES, Molloy K, Colucci AM (2003) The use of hexamethyldisilathiane for the synthesis of transition metal sulfides. Polyhedron 22:1255–1262

Choi J, Gillan EG (2005) Solvothermal synthesis of nanocrystalline copper nitride from an energetically unstable copper azide precursor. Inorg Chem 44:7385–7393

Fabbricatore P, Fernandes P, Gualco GC, Merlo F, Musenich R, Parodi R (1989) Study of niobium nitrides for superconducting r.f. cavities. J Appl Phys 66:5944–5949

Fenker M, Balzer M, Buchi RV, Jehn HA, Kappl H, Lee JJ (2003) Deposition of NbN thin films onto high-speed steel using reactive magnetron sputtering for corrosion protective applications. Surf Coat Technol 163:169–175

Fischer A, Antonietti M, Thomas A (2007) Growth confined by the nitrogen source: synthesis of pure metal nitride nanoparticles in mesoporous graphitic carbon nitride. Adv Mater 19:264–267

George PP, Gedanken A (2008) Synthesis, characterization, and photoluminescence properties of In_2O_3 nanocrystals encapsulated by carbon vesicles and neat In_2O_3 nanocrystals generated by the RAPET technique. Eur J Inorg Chem 6:919–924

George PP, Pol VG, Gedanken A (2007) Synthesis and characterization of Nb_2O_5@C core-shell nanorods and Nb_2O_5 nanorods by reacting $Nb(OEt)_5$ via RAPET (reaction under autogenic pressure at elevated temperatures) technique. Nanoscale Res Lett 2:17

Gillan EG, Kaner RB (1994) Rapid solid-state synthesis of refractory nitrides. Inorg Chem 33:5693–5700

Gispert MP, Serro AP, Colaço R, Botelho do Rego AM, Alves E, daSilva RC, Brogueira P, Pires E, Saramago B (2007) Tribiological behaviour of Cl-implanted TiN coatings for biomedical applications. Wear 262:1337–1345

Gomathi A, Rao CNR (2006) Nanostructures of the binary nitrides, BN, TiN, and NbN, prepared by the urea-route. Mater Res Bull 41:941–947

Griffiths LE, Mount AR, Pulham CR, Lee MR, Kondoh H, Ohta T (2001) Low temperature electrochemical synthesis of titanium nitride. Chem Commun 6:579–580

Hector AL, Parkin IP (1995) Sodium azide as a reagent for solid state metathesis preparations of refractory metal nitrides. Polyhedron 14:913–917

Hershfinkel M, Gheber LA, Volterra V, Hutchison JL, Margulis L, Tenne R (1994) Nested polyhedra of MX_2 (M = W, Mo; X = S, Se) probed by high-resolution

electron microscopy and scanning tunneling microscopy. J Am Chem Soc 116:1914–1917

Hu J, Lu Q, Tang K, Yu S, Qian Y, Zhou G, Liu X, Wu J (2000) Low-temperature synthesis of nanocrystalline titanium nitride via a benzene-thermal route. J Am Ceram Soc 83:430–432

Joshi UA, Chung S-H, Soo Hyun J-S, Lee (2005) Low-temperature, solvent-free solid-state synthesis of single-crystalline titanium nitride nanorods with different aspect ratios. J Solid State Chem 178:755–760

Li YG, Gao L (2003) Synthesis and characterization of nanocrystalline niobium nitride powders. J Am Ceram Soc 86:1205–1207

Margulis L, Salitra G, Talianker M, Tenne R (1993) Nested fullerene-like structures. Nature 365:113–114

O'Loughlin JL, Wallace CH, Knox MS, Kaner RB (2001) Rapid solid-state synthesis of tantalum, chromium, and molybdenum nitrides. Inorg Chem 40:2240–2245

Ostling M, Nygren S, Petersson CS, Norstrom H, Buchta R, Blom HO, Berg S (1986) A comparative study of the diffusion barrier properties of TiN and ZrN. Thin Solid Films 145:81–88

Pol SV, Pol VG, Gedanken A (2004a) Reactions under autogenic pressure at elevated temperature (RAPET) of various alkoxides: formation of metals/metal oxides-carbon core-shell structures. Chem Eur J 10:4467–4473

Pol VG, Pol SV, Gedanken A, Goffer Y (2004b) Thermal decomposition of tetraethylorthosilicate (TEOS) produces silicon coated carbon spheres. J Mater Chem 14:966–969

Pol SV, Pol VG, Kessler VG, Seisenbaeva GA, Sung M, Asai S, Gedanken A (2004c) The effect of a magnetic field on a RAPET (reaction under autogenic pressure at elevated temperature) of $MoO(OMe)_4$: fabrication of MoO_2 nanoparticles coated with carbon or separated MoO_2 and carbon particles. J Phys Chem B 108:6322–6327

Pol SV, Pol VG, Kessler VG, Gedanken A (2006) Growth of carbon sausages filled with in situ formed tungsten oxide nanorods: thermal dissociation of tungsten(VI) isopropoxide in isopropanol. New J Chem 30:370–376

Storms EK (1972) Contribution to phase relationships and electrical properties of refractory carbides and nitrides. Solid State Chem. MTP International Review of Science, University Press, 10:37–38

Sundgren JE (1985) Structure and properties of TiN coatings. Thin Solid Films 128:21–44

Tenne R (1995) Doped and heteroatom-containing fullerene-like structures and nanotubes. Adv Mater 7:965–995

Tenne R, Margulis L, Genut M, Hodes G (1992) Polyhedral and cylindrical structures of tungsten disulphide. Nature 360:444–446

Toth LE (1971) Transition metal carbides & nitrides. In: Refractory materials, vol 7. Academic Press, New York

Troitskiy VN, Domashnev IA, Kurkin EN, Grebtsova OM, Berestenko VI, Balikhin IL, Gurov SV (2003) Synthesis and characteristics of ultra-fine superconducting powders in the Nb–N, Nb–N–C, Nb–Ti–N–C systems. J Nanopart Res 5:521–528

Wu H, Hunting J, Uheda K, Lepak L, Konkapaka P, Disalvo FJ, Spencer MG (2005) Rapid synthesis of gallium nitride powder. J Cryst Growth 279:303–310

Zhang QH, Gao L (2004) Ta_3N_5 nanoparticles with enhanced photocatalytic efficiency under visible light irradiation. Langmuir 20:9821–9827